THE PUBLISHING HOUSE
OF THE ROMANIAN ACADEMY

PROCEEDINGS OF THE ROMANIAN ACADEMY, Series A,
Volume 26, Number 4/2025, pp. 375–383
DOI: 10.59277/PRA-SER.A.26.4.06

SPECTRAL BASED SEGMENTATION AND BIO-OPTICAL DESCRIPTORS OF CELLS FROM SEROUS CAVITY EFFUSION

Ana-Maria PLEAVA[1], Mihaela-Andreea ILISANU[2], Mona MIHAILESCU[3], Eugen SCARLAT[4], Alina GHIOCA[5], Andrei UNGUREANU[6], Ion Gabriel VLADU[6], Darius-Mihail CRISTEA[6], Vlad FECHETE[6], Nicolae TARBA[4], Elena TIANU[5], Valentin POPESCU[5], Gabriela VULPOIU[7], Mihaela-Georgeta MOISESCU[8], Violeta Liuba CALIN[1,8]

[1] Politehnica University of Bucharest, QOPTE Laboratory, CAMPUS Research Institute, Bucharest, Romania
[2] Politehnica University of Bucharest, Comp. Sci. Eng. Dept., Comp. Sci. Doct. School. Fac. of Autom. Contr. and Comp., Romania
[3] Politehnica University of Bucharest, Applied Sciences in Engineering Research Center, Romania
[4] Politehnica University of Bucharest, Physics Dept., Romania
[5] Imunomedica Provita SRL, Bucharest, Romania
[6] Politehnica University of Bucharest, Applied Sciences Faculty, Romania
[7] Politehnica University of Bucharest, Medical Engineering Faculty, Romania
[8] Biophys. Univ. Med. Pharm. Carol Davila, Cell. Biotech. Dept, Excell. Cent. Res. Biophys. Cell. Biotech, Bucharest, Romania
Corresponding author: Mihaela-Andreea ILISANU, E-mail: mihaela.ilisanu@upb.ro

Abstract. Serous cavity effusions provide valuable information for both cancer diagnosis and therapy. Conventional analysis relies on cytological examination, when nuclear/cytoplasmic morphology and coloration are evaluated under brightfield microscopy. In this study, we examined malignant and benign cells from serous cavity effusions using high-content hyperspectral microscopy. We propose several criteria for cells and cellular subcomponents segmentation based on spectral profiles. Differences were found between biophysical descriptors computed for the cytoplasm and nuclei of malign/benign cells. We demonstrate the possibility to extract quantitative information on bio-optical properties of cytology specimens, to be used further for an automate classification based on hyperspectral microscopy images.

Keywords: hyperspectral images, cells descriptors, serous cavity effusion, spectral curves and vectors, segmentation, bio-optical descriptors, subcellular level.

1. INTRODUCTION

The use of high-content imaging techniques for extraction of features with biophysical significance offers important sources of information for medicine and biology. Hyperspectral microscopy (HYS) is an example of this type of technique that captures the cells' optical signatures, which reflect both morphological, and biochemical properties at the subcellular level [1]. The spectral information measured by HYS is related to both phenomena: scattering and absorption of light within the sample [2]. HYS, a mix of microscopy with spectroscopy, produces a hyperspectral data cube, a multi-dimensional image (HYSI) having in each pixel detailed intensity information between 400 nm–1000 nm [3]. Enhanced darkfield hyperspectral microscopy is a HYS configuration that augments the image contrast and optimizes the signal-to-noise ratio. The resulted scattered light profiles serve as unique spectral fingerprints reflecting molecular composition, structural organization, and other biophysical properties of cellular compartments. It is considered thus a rich source of information with the potential to transform cytological imaging into a high-dimensional information acquisition process.

It has been already used in different biomedical domains: hematology [4], cancer detection and diagnosis [5–7] irradiated radioresistant cells [8], endoscopy and minimally invasive surgery [9], and neurology to diagnose Alzheimer's disease via the retina [10, 11]. Information provided at the subcellular level was also used for the study of the interaction of cells with nanomaterials: subcellular localization and uptake efficiency of different gold and silica nanoparticles in human cells lines (A549, HepG2 and Caco2) [12, 13] metallic nanoparticles incorporation and internal traffic in murine embryonic fibroblast cell line [14], carbon nanodots penetration inside nucleus [15]. Hashimoto et al. demonstrated that HYSI outperform conventional RGB imagery [16], by using a pixel-wise classification method over H&E stained liver samples, employing

simultaneously spatial and spectral features for detecting five liver tissue components: nucleus, sinusoid, lymphocytes, fibers and cytoplasm. Additionally, the capabilities of HYS to measure colors accurately was used as standard to measure staining performance. For example, Yagi et al. used a standardized color chart [17] to propose a method for color validation and optimization based on whole slide images. This procedure is considered a promising solution for the biggest challenge represented by the variations in appearance of H&E stained slide from different laboratories when using whole slide imaging. Related with this, Salehen et al. evaluated the color performance of two different whole-slide imaging systems using HYSI and three different H&E stained histological samples as color targets [18].

Extraction of features with biomedical relevance is an indispensable aspect of modern image processing tools, supporting automation of decision-making processes [19, 20]. Handcrafted features are preferred by biomedical scientists being closely associated with the characteristics of the investigated sample and interpreted in a clinical context [21]. HYSI allows various categories of features: spatial-spectral [22, 23], textural and morphological [24], physiological/biochemical [25], obtained from spectral profiles at single pixel level [26], or used for entire individual tumor cells [27].

Cells from cavity serous effusions are clinically significant specimens that provide valuable information for the management of malignant diseases [28]. Cytological examination is essential first of all to conduct the screening [29]. Conventional diagnostic workflows rely on brightfield microscopy evaluation of nuclear and cytoplasmic morphology on stained smears, by trained Pathologists [30]. In this conventional approach, much of the cells intrinsic biophysical information is left unexploited. Appropriate and dedicated tools for cells segmentation can be used to extract biophysical properties and differentiate malignant from benign cells with bio-optical descriptors of distinct sub-cellular compartments [31].

In the case of HYSI, cell segmentation addresses unique challenges due to its multi dimensionality. The utility of segmentation methods in HYSI was already demonstrated for: nuclei and cytoplasm of white blood cells using spectral angle mapper SAM [32], glandular structures of prostate cancer based on Gleason grade [33], mitotic cell candidate regions by the Bayesian modeling and local-region threshold method [34].

In this study, we proposed and compared multiple segmentation criteria for nucleus–cytoplasm separation in HYSI of cells from serous cavity effusions. Pixel-level spectral profiles (SPs) were considered as curves and vectors; segmentation criteria were based on intensity ratios at selected wavelengths, statistical descriptors of intensity distributions, areas under spectral curves, and distances between spectral vectors. Thousands of reference SPs were collected allowing extracting various compartment-specific bio-optical descriptors – such as statistical distributions of spectral intensity values, spectral curve integrals, and texture features – that can serve as discriminative variables for further automate classification or computational modeling of cells.

2. SAMPLES PREPARATION AND IMAGES ACQUISITION

2.1. Samples preparation

A surgeon under sterile conditions performed cavity serous fluid collection from patients who signed informed consent. After enrichment by centrifugation, the cellular sediment was transferred into BD SurePath vials. Using the BD TriPath Imaging equipment and BD Settling sedimentation chambers, after additional centrifugation, decantation, and washing steps, cells were deposited (10 min sedimentation time) in monolayer on slides. Slides were washed with distilled water, immersed for 20 min in 95% ethanol and stained using the Papanicolaou (PAP) protocol (Harris Hematoxylin as nuclear stain, and Orange G and EA 50 as cytoplasmic stains). An experienced Pathologist examined the slide in brightfield microscopy and create a map indicating the presence of malignant (Mc) and benign (Bc) cells to be used for HYSI recording.

2.2. Hyperspectral images and spectral profiles

The spectral data were acquired using a Cytoviva enhanced darkfield hyperspectral microscope [35]. The system provides illumination at a very oblique angle using an oil-immersed cardioid- shaped condenser and a light guide with liquid core, a configuration that enhances high contrast images, achieves a signal-to-noise ratio up to 10 times higher than that of conventional dark field optics. Illumination was provided by a white light source (FiberLite DC-950, 150 W quartz halogen, Dolan Jenner Industries, USA). Images were recorded

using a visible to near-infrared spectrophotometer (ImSpectrum V10E, SPECIM, Finland, with spectral range 400–1000nm, 1.5nm resolution) placed in front of a CCD camera (1392 × 1040pixels, 6.45µm pixel size, 7.3–13.5 fps, 5 µs–60 s exposure). Automated transversal scanning was performed using a NanoScanZ 400 module (Prior Scientific Instruments Ltd., UK) to acquire HYSI data line by line. This procedure provides unique scattered light profiles and quantitative spectral information useful to discriminate between different cells components [36]. Data visualization and analysis were conducted in ENVI software.

3. SEGMENTATION CRITERIA AND CELLS DESCRIPTORS

Figure 1 presents the conceptual workflow for extracting biophysical information from HYSI of cells. The main steps are: 1) sample preparation; 2) Mc identification and slide map drawing by our Pathologist; 3) recording of HYSIs; 4) collection of the reference SPs; 5) application of SAM ENVI to build the spectral library; 6) identification of significant spectral points (local maxima/minima, inflexion points); 7) computation of parameters on SPs; 8) design and application of the segmentation criteria (C1-C4 described below); 9) display of the masks for nucleus and cytoplasm; 10) computation of weights to compare the efficacy of segmentation criteria; 11) combination of the segmentation criteria and display of second-generation masks; 12) computation of the geometrical features and their distributions; 13) split of the dataset in Mc/Bc; 14) extraction of compartment-specific bio-optical descriptors.

It is noteworthy that the segmentation criteria rely on SPs taken together for Mcs and Bcs. Cells were annotated at a later stage as benign and malign as explained below, according to size distribution.

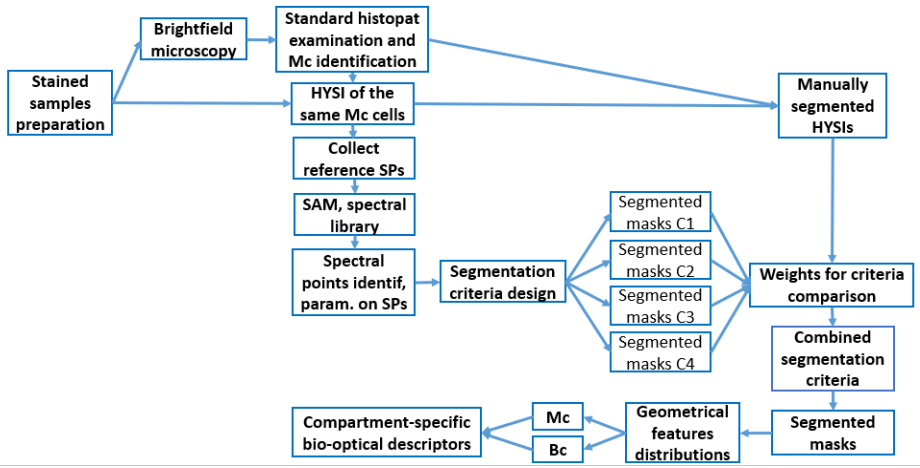

Fig. 1 – Conceptual workflow of the procedure of extracting biophysical information from HYSIs of cells from serous cavity.

3.1. Images preprocessing

Figure 2 presents examples of images of the same area of a slide with PAP-stained cells in a) brightfield microscopy and b) HYS. One may observe the larger dimensions and the hyperchromatic nucleus of the Mc from the image center compared to the Bcs around it.

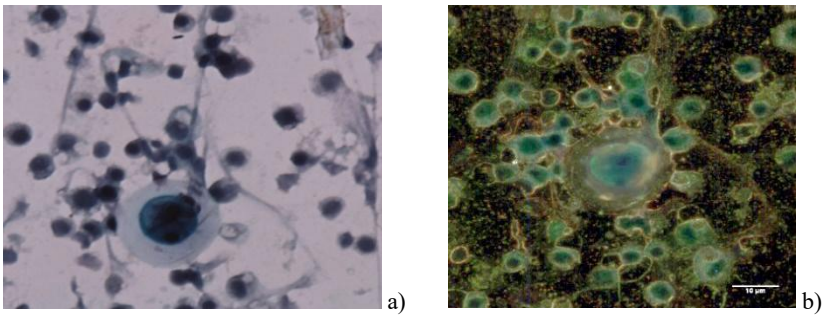

a) b)

Fig. 2 – Example of a Mc and many Bcs in brightfield image (a) and in the corresponding HYSI (b) for the same slide area.

Three reference libraries containing SPs selected using SAM procedure were developed for each nucleus, cytoplasm and background classes. Examples of SPs are presented in Fig. 3 (as an average on 10×10 pixels).

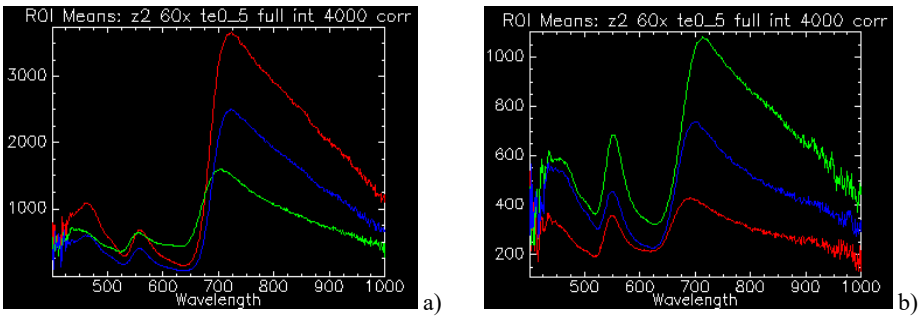

Fig. 3 – Examples of reference spectral profiles of: a) average 10×10 pixels for nucleus; b) average 10×10 pixels for cytoplasm.

The following steps were used in developing a reference library: a) lamp correction of HYSI, using a dark image recorded with blocked illumination; b) collection of SPs using ENVI software, by a simple click on a pixel from nucleus/cytoplasm/background regions; c) checking of each reference SP for its representativeness by applying the SAM procedure in ENVI software; d) normalization of each SP by dividing at the maximum value in MATLAB script; e) computation of SPs as an average on 10×10 pixels (to reduce the background noise) using the ROI function. More details about SP pre-processing are in [22]. The reference spectra were analyzed with SAM procedure [14]. Only SPs with highest values of similarity (0.12 radians angle between spectra) were included in each spectral library.

A MATLAB script was developed to perform several operations on reference SPs prior to segmentation criteria: identification of significant spectral points (local maxima/minima, inflexion points), separation of spectral channels, computation of intensity ratios and building of histograms for SP distributions on each class.

Local maxima were identified for red (720nm), green (560nm), and blue (460 nm), the highest intensity values being found in the red part of the spectrum. We computed intensity ratios: intensity at red maximum / intensity at green maximum I_{red}/I_{green}, intensity at red maximum / intensity at blue maximum I_{red}/I_{blue}, and intensity at green maximum / intensity at blue maximum I_{green}/I_{blue}. Figure 4 presents three sub-images on red, green, and blue spectral bands identified above. For further calculations, three spectral channels were defined as follows: red (685–737 nm), green (550–575 nm), and blue (455–470 nm).

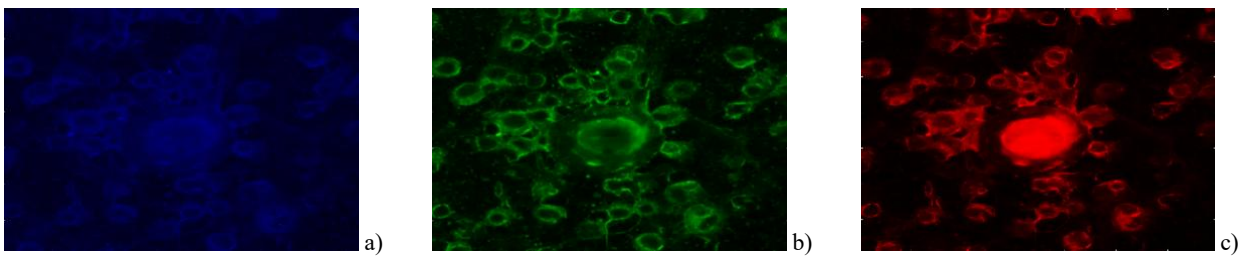

Fig. 4 – Examples of sub-images on spectral bands: a) blue (460 nm); b) green (560 nm); c) red (720 nm).

3.2. Segmentation criteria

The reference SPs collected were exported as annotated data for pixel-wise classification process in three classes (nucleus, cytoplasm, background). Next, the normalized SPs were considered as functions (to compute areas under curves, ratios of local maxima intensities), as 468-dimensional vectors (to compute Euclidean distances and angles in vector space), and as statistical distributions of intensity values in a class (to compute skewness and kurtosis per class). Based on these values (computed as average and standard deviations on each class), the following criteria for segmentation were designed:

C1 (intensity ratio) applied as follows: pixels with ratio $I_{red}/I_{green}>3$ were allocated to the nucleus, pixels with that ratio smaller than 3 to the cytoplasm, while pixels without the three maxima in SPs and with intensity values below ¼ from the average intensity of the whole image were assigned to the background.

C2 (*skewness of intensity values distribution*), specifically only Skewness values on red channel were found different and used to classify pixels into the three classes.

C3 (*spectral area under SP*), computed on the three spectral channels, for which only the red channel was considered, using threshold values established by comparison with the manually segmented cells.

C4 (*spectral distance*). To detect the pixels having SP similar to the reference ones, we built the spectral distance mapper application (SDMA) a dedicated interface to convert an image into a map where the colors represent the distance between the SP of each pixel and the reference SP (an example is in [37]). Smaller distance values indicate pixels that exhibit a SP similar to the reference. Two threshold values for nucleus and cytoplasm were chosen by the user, the rest being considered as background.

By applying each criterion, masks with three colors (black for background, yellow for cytoplasm, red for nucleus) were provided. The segmented shapes were then filled using the built-in *alpha shape* function from MATLAB, as described in [14]. We compared the criteria performance by calculating the weight (W) of correctly classified pixels using manually segmented HYSIs as the ground truth.

3.3. Bio-optical descriptors

In contrast with classical optical microscopy, modern digital methods provide multiple and complex information linked with cells/ tissues biophysical properties: super-resolution [38], second harmonic generation [39], holographic [40, 41], diffraction phase [42] microscopies.

In our case, the nuclei and cytoplasm of Mcs and Bcs segmented from HYSIs were further considered to compute four type of bio-optical descriptors: (i) geometrical features (projected area, major, and minor axis) computed using *regionprops* function from MATLAB, by exploiting the size criteria used in diagnostic cytology [43]; (ii) spectral features (the ratio of maximum intensities on the three spectral bands and the area under the curve on the three spectral channels) computed considering SPs as functions; (iii) texture features (Contrast, Correlation, Energy, Homogeneity) computed by using intensity values through neighbor pixels; (iv) statistical features (mean, skewness, and kurtosis) computed from histograms of intensities on spectral channels of SPs collected from fully segmented areas.

4. RESULTS AND DISCUSSION

The SPs (selected using the SAM procedure) as references for nucleus and cytoplasm (Fig. 3) showed three main peaks of scattered light centered on the following maxima in blue (460 nm), green (560 nm), and red (720 nm). These maxima are difficult to attribute to specific cellular components (nucleic acids, keratin, positively charged proteins, etc.) considering that our cells were PAP stained. PAP is a polychromatic stain, using multiple dyes with broad, overlapping spectra to create the visual contrast helping the pathologist in cell evaluation. Nevertheless, a quantitative analysis of these spectra may be exploited for identification of pixels corresponding to specific cellular structures (nucleus, cytoplasm, parts of cytoplasm) allowing their segmentation. Criteria for such segmentation are thus provided.

We previously presented [37] examples of images where specific segmentation criteria were used and concluded that a combination of such criteria is needed for a realistic segmentation; here we worked on a larger data set (three patients). To compare segmentation criteria between them, their similitude with a manual segmentation were quantified by computing: 1) W_N – the ratio of the number of segmented pixels belonging to nuclei to the total number of nuclei pixels in the reference image, 2) W_C – the ratio of the number of segmented pixels belonging to cytoplasm to the total number of cytoplasm pixels in reference image, and 3) W_T – the ratio of the number of segmented pixels to the total number of pixels in the reference image. As can be seen in Table 1, the best W_N was obtained with C1, while the highest value for W_C was obtained with C4.

Table 1

Weights of pixels segmented using C1, C2, C3, C4 criteria and their combination

	W_T	W_N	W_C
C1	67.30	86.88	52.15
C2	41.45	56.23	73.29
C3	41.15	0.15	49.21
C4	79.44	57.59	77.35
C1+C4	79.17	88.58	81.07

In Figs. 5a and 5b, there are several examples of segmented cells using the combination of C1 and C4 followed by the filling procedure. We observed very good results for nuclei but not for cytoplasm, as Mcs were positioned in clusters with Bcs or cellular fragments. In brightfield microscopy images, the main causes of errors in cytoplasm segmentation are cell clustering and overlapping, specular reflection or halos, the weak staining and faint and blurred boundaries of cytoplasm, and many more. In case of HYSI, the spectral criteria which are at the core of the segmentation method correctly recognizes and correctly assigns pixels as part of the cytoplasm and not the nucleus or background, but does not separate cells from each other, the reported errors being caused by the cell overlapping. This problem of separating objects in an image where they are adjacent or overlapping is old in segmentation, reported in many cases and for which several functions have been proposed (edge detection, watershed, filters, etc.), but remains a challenge for images from experimental samples no matter the optical techniques used for microscopy.

For the computation of the bio-optical descriptors only nuclei were further considered (Fig. 5c) together with the perinuclear cytoplasm, defined as a 15 pixel-annulus around nuclei (Fig. 5d).

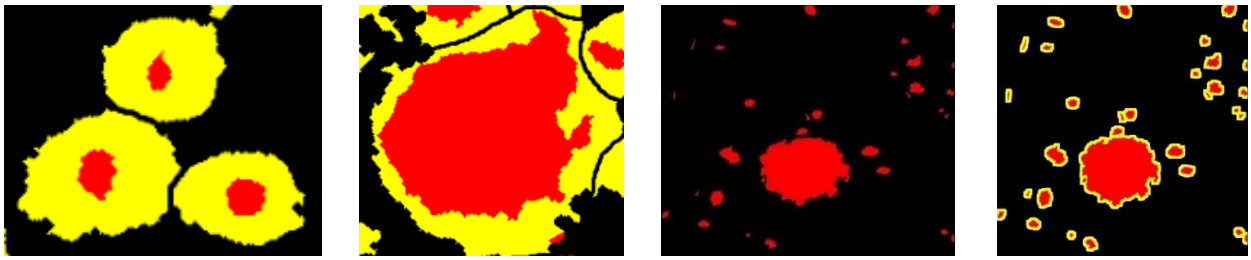

a) b) c) d)

Fig. 5 – Examples of masks with segmentations based on combined C1 and C4 for Bc (a) Mc (b); only nuclei (c) nuclei and the perinuclear ring of cytoplasm (d).

Figure 6 a presents an example of distribution of the projected area of nuclei (approx. 200 Bc nuclei and 20 Mc nuclei). As there is a clearly bimodal distribution, separated by a large interval, nuclei have been easily distributed and counted, according to their large or small size as malign/benign. This label was preserved for all further computation of bio-optical descriptors on cells. Geometrical features (projected area, minor axis, major axis) for nuclei of Mcs and Bcs were computed as ratios N_Mc/N_Bc (Fig. 6b). It is observed that malignant nuclei have areas over 50 times larger and axes over approximately 10 times larger than benign ones. Given this large difference between geometrical features, we consider them suitable to be used as a size-based filter step for separation in Mc and Bc nuclei prior to the calculation of the bio-optical descriptors for an automatic separation.

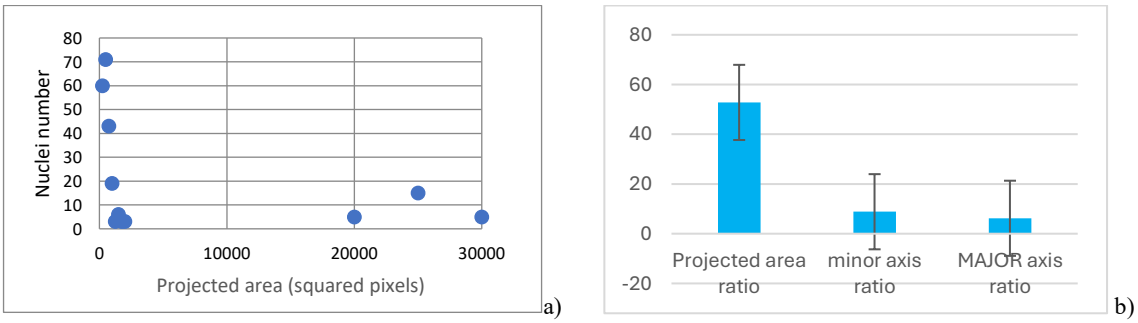

a) b)

Fig. 6 – (a) Distribution of nuclei projected area and (b) projected area, minor and major axis computed as ratio N_Mc/N_Bc.

Figure 7 (a and b) presents the following spectral features computed on the chosen spectral channels for nuclei and peripheral cytoplasm: intensity ratios on spectral bands (Fig. 7a) and areas under curves on spectral channels (Fig. 7b). It is observed from Fig. 7a that for both malignant and benign nuclei the red/green and red/blue intensity ratios are greater than 3 (this finding being already used as C1 criterion to separate nuclei from cytoplasm). The intensity value for the red channel of N_Mc is almost 3 times higher than for the red channel of N_Bc (Fig. 7b). This means in the case of our samples a larger amount of dye, which binds to chromatin, accumulated in N_Mc, demonstrating a higher accumulation of genetic material. These spectral

features, initially used for segmentation, are also considered suitable for automatic cell classification due to the significant differences observed between the two types of nuclei.

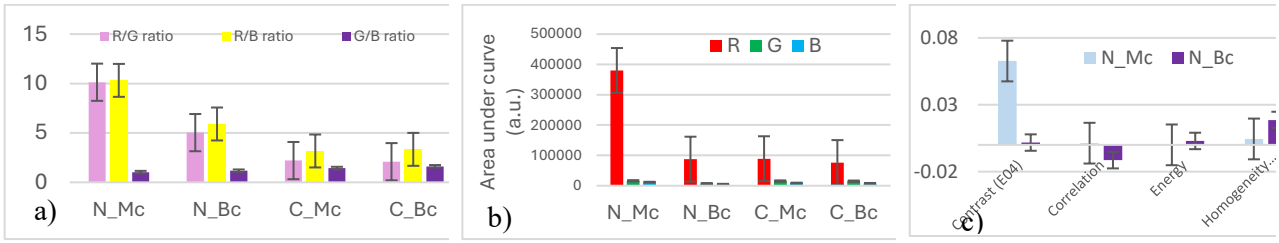

Fig. 7 – Spectral features: a) intensity ratios at RGB spectral bands; b) areas under curve at RGB channels and c) texture features.

Figure 7c presents the texture features computed only for nuclei, as in the case of the peripheral cytoplasm it has no significance. Different values between the nuclei of the two cell types were only observed for Contrast parameter. The texture features reflect the object's surface structure and heterogeneity in internal organization, providing information beyond color and shape (spectral and spatial), helping to identify patterns and structures within an image, crucial for tasks like image segmentation, classification, and analysis in computer vision and medical imaging [44].

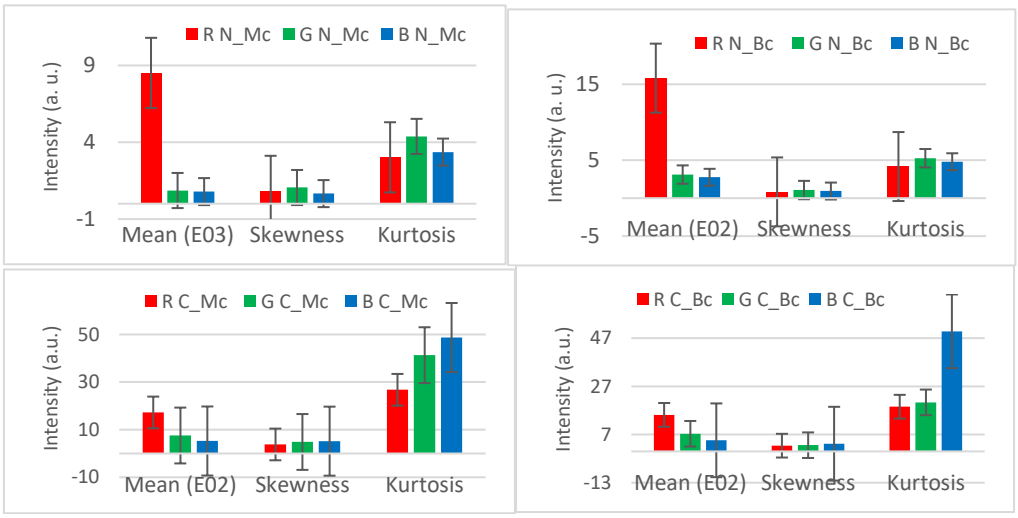

Fig. 8 – Statistical features based on SPs intensity computed for Mc and Bc nuclei (top raw) and cytoplasm (bottom raw)

Figure 8 presents the statistical features computed based on intensity values on the spectral channels. It can be observed that all statistical parameters (Mean, Skewness, and Kurtosis) exhibit differences between the four classes.

We found that among the investigated descriptors, intensity ratios red/green, area under curve for red channel, and contrast were different between nuclei of Mcs and Bcs, being possible their employment in segmentation.

Since we worked with Pap stained samples, the spectral fingerprint is correlated to the optical properties of the colorants that binds in different amounts to specific molecules of the nucleus/cytoplasm and therefore the spectral profiles for the nucleus/cytoplasm (Fig. 3), although they show maxima at the same wavelengths, have different intensities. This allowed the formulation of the C1 criterion and bio-optical descriptors based on spectral information that in other microscopy techniques do not exist over such a wide range (400–1000nm).

Our findings are to be interpreted in the context of cells' malignant transformation, which modifies the staining features of the cell, mainly at the nucleus level. In standard cytology, for the nucleus, there are several hallmarks of malignancy like hyperchromasia, pleomorphism (irregular contour and chromatin distribution, prominent nucleoli), nuclear enlargement and increased nuclear-to cytoplasm ratio, while modification of cytoplasmic features (scant and altered staining of cytoplasm, vacuolization) is generally less specific than the nuclear ones [27, 28]. Considering this, we assume that differences between the spectral optical descriptors for

Mcs and Bcs could result especially from the quantity and organization of chromatin [45]. Spatial-spectral features were used before to differentiate between normal, dysplastic and squamous cell carcinoma cervical cells with good accuracy [46]. Compared with standard histological evaluation, our method offers a significant advantage through the extensive spectral information (400–1000 nm) acquired from each cell enabling more detailed cellular characterization.

CONCLUSIONS

This work presents a simple method for segmentation of cells and cell components from HYSI of stained cytology samples from cavity serous fluids. Several criteria based on spectral profiles were used to perform nuclei-cytoplasm separation and four types of bio-optical descriptors were computed.

We demonstrated that the investigation of the cells from serous fluid in HYS, combining conventional imaging and spectrophotometry, yields high-content data and together the spatial and spectral features and provides criteria for segmentation, in the view of a comprehensive characterization of cells across various pathological states. Our approach reframes cytology as an information extraction challenge: the goal is not only to visualize cells but also to translate their spectral-biophysical signatures into structured, analyzable data, to serve as a rich, quantitative basis for an automate decision-making process in clinical and research contexts.

ETHICAL STATEMENT

This study was approved by the ethical committee of the Imunomedica Provita SRL.

ACKNOWLEDGEMENTS

This work was supported by research project 8PED/2025, PN-IV-P7-7_1-PED-2024-1895. Hyperspectral imaging was possible due to European Regional Development Fund through Competitiv. Operational Program 2014-2020, Priority axis 1, INOVABIOMED.

REFERENCES

[1] Oladipo AO, et al. Bimetallic Au@Pd nanodendrite system incorporating multimodal intracellular imaging for improved doxorubicin antitumor efficiency. Int. J. Pharm. 2021; 602: 120661. DOI: 10.1016/j.ijpharm.2021.120661.
[2] Ortega S, et al. Hyperspectral and multispectral imaging in digital and computational pathology: a systematic review. Biomed Opt Express. 2020; 11: 3195–3233. DOI: 10.1364/BOE.386338.
[3] Lu G, Fei B. Medical hyperspectral imaging: a review. J. Biomed. Opt. 2014; 19: 010901. DOI: 10.1117/1.JBO.19.1.010901.
[4] Verebes GS, et al. Hyperspectral enhanced dark field microscopy for imaging blood cells. J. Biophotonics. 2013; 6: 960–967. DOI: 10.1002/jbio.201300067.
[5] Liu L, et al. Staging of skin cancer based on hyperspectral microscopic imaging and machine learning. Biosens. 2022; 12: 790. DOI:10.3390/bios12100790.
[6] Kho E, et al. Broadband hyperspectral imaging for breast tumor detection using spectral and spatial information. Biomed. Opt. Express. 2019; 10, 4496–4515. DOI:10.1364/BOE.10.004496.
[7] Manea R, et al. A method for assessing mammary tumours based on hyperspectral imaging. Romanian Reports in Physics. 2015; 67: 1503−1511.
[8] Tudor M, et al. In vitro hyperspectral biomarkers of human chondrosarcoma cells in nanoparticle-mediated radiosensitization using carbon ions. Sci. Reports. 2023; 13(1): 14878. DOI: 10.1038/s41598-023-41991-9.
[9] Yoon J, et al. A clinically translatable hyperspectral endoscopy (HySE) system for imaging the gastrointestinal tract. Nat. Commun. 2019; 10(1): 1902. DOI: 10.1038/s41467-019-09484-4.
[10] Hadoux X, et al. Non-invasive in vivo hyperspectral imaging of the retina for potential biomarker use in Alzheimer's disease. Nat. Commun. 2019; 10(1): 4227. DOI: 10.1038/s41467-019-12242-1.
[11] More SS, et al. In vivo assessment of retinal biomarkers by hyperspectral imaging: early detection of Alzheimer's disease. ACS Chem. Neurosci. 2019; 10: 4492–4501. DOI: 10.1021/acschemneuro.9b00331.
[12] Sohrabi Kashani A, Piekny A, Packirisamy M. Using intracellular plasmonics to characterize nanomorphology in human cells. Microsystems Nanoeng. 2020; 6: 110. DOI:10.1038/s41378-020-00219-w
[13] Miclea LC, et al. Evaluation of intracellular distribution of folate functionalized silica nanoparticles using fluorescence and hyperspectral enhanced dark field microscopy. Nanoscale. 2022; 14: 12744–12756. DOI:10.1039/D2NR01821G
[14] Mihailescu M, et al. Method for nanoparticles uptake evaluation based on double labeled fluorescent cells scanned in enhanced darkfield microscopy. Biomed. Opt. Express. 2023; 14: 2796–2810. DOI: 10.1364/BOE.490136.

[15] Zhang W, et al. Dark-field microscopic study of cellular uptake of carbon nanodots: nuclear penetrability. Molecules. 2022; 27: 2437. DOI: 10.3390/molecules27082437.
[16] Hashimoto E, et al.Tissue classification of liver pathological tissue specimens image using spectral features. In: Proceedings SPIE, vol. 10140. Medical Imaging: Digital Pathology. 2017, p. 101400Z. DOI:10.1117/12.2253818.
[17] Cheng WC, Saleheen F, Badano A. Assessing color performance of whole-slide imaging scanners for digital pathology. Color Res. Appl. 2019; 44: 322–334. DOI: 10.1002/COL.22365.
[18] Yagi Y. Color standardization and optimization in Whole Slide Imaging. Diagn. Pathol. 2011; 6: S15. DOI: 10.1186/1746-1596-6-S1-S15.
[19] Calin VL, et al. Grading of glioma tumors using digital holographic microscopy. Heliyon. 2024; 10: 9. DOI: 10.1016/j.heliyon.2024.e29897.
[20] Rundo L, Militello C. Image biomarkers and explainable AI: handcrafted features versus deep learned features. Eur. Radiol. Exp. 2024; 8(1): 130. DOI: 10.1186/s41747-024-00529-y.
[21] Da F. Mendes CFS, Krohling RA. Deep and handcrafted features from clinical images combined with patient information for skin cancer diagnosis. Chaos, Solitons & Fractals. 2022; 162: 112445. DOI:10.1016/j.chaos.2022.112445.
[22] Negoita RD, et al. Specific spectral sub-images for machine learning evaluation of optical differences between carbon ion and X ray radiation effects. Heliyon. 2024; 10: e35249. DOI: 10.1016/j.heliyon.2024.e35249.
[23] Fabelo H, et al. Spatio-spectral classification of hyperspectral images for brain cancer detection during surgical operations. PLoS One. 2018; 13: e0193721. DOI: 10.1371/journal.pone.0193721.
[24] Thibault G, Angulo J, Meyer F. Advanced statistical matrices for texture characterization: application to cell classification. IEEE Trans. Biomed. Eng. 2014; 61: 630–637. DOI: 10.1109/TBME.2013.2284600.
[25] Lucas A, et al. Hyperspectral wide-field-of-view imaging to study dynamic microcirculatory changes during hypoxia. Am. J. Physiol. Heart Circ. Physiol. 2022; 323: H49–H58. DOI: 10.1152/ajpheart.00624.2021.
[26] Tarba N, et al. Distance between species by confusion operators of multi-class classifiers. U.P.B. Sci. Bull., Ser. A. 2025; 87: 171–182.
[27] Uhr JW, et al. Molecular profiling of individual tumor cells by hyperspectral microscopic imaging. Transl. Res. 2012; 159: 366–375. DOI: 10.1016/j.trsl.2011.08.003.
[28] Li M, et al. Detection of carcinoma in serous effusions. Am. J. Cancer Res. 2021; 11: 43–60.
[29] Wang C, et al. Multiple serous cavity effusion screening based on smear images using vision transformer. Sci. Rep. 2024; 14(1): 7395. DOI: 10.1038/s41598-024-58151-2.
[30] Huang C, et al. Minimally invasive cytopathology and accurate diagnosis: technical procedures and ancillary techniques. In Vivo. 2023; 37: 11-21. DOI: 10.21873/invivo.13050.
[31] Jermain PR, et al. Deep learning-based cell segmentation for rapid optical cytopathology of thyroid cancer. Sci. Rep. 2024; 14(1): 16389. DOI: 10.1038/s41598-024-64855-2.
[32] Li Q, Wang Y, Liu H, Wang J, Guo F. A combined spatial-spectral method for automated white blood cells segmentation. Opt. Laser Technol. 2013; 54: 225–231.
[33] Zarei N, et al. Automated prostate glandular and nuclei detection using hyperspectral imaging. In: Proc. of 14th Int. Symp. Biomed. Imaging. 2017, pp. 1028–1031.
[34] Lu C, Mandal M. Toward automatic mitotic cell detection and segmentation in multispectral histopathological images. IEEE J. Biomed. Heal. Informatics. 2014; 18: 594–605. DOI: 10.1109/JBHI.2013.2277837.
[35] CytoViva, Hyperspectral microscope. User Manual. https://cytoviva.cn/wp-content/uploads/2021/pdf/CytoViva-User-Manual_10022020.pdf [accessed September 15, 2025].
[36] Ortega S, et al. Detecting brain tumor in pathological slides using hyperspectral imaging. Biomed. Opt. Express. 2018; 9: 818. DOI: 10.1364/BOE.9.000818.
[37] Ilisanu MA, et al. Spectral criteria for automated segmentation of cells from cavity serous fluids. In: 48th International Semiconductor Conference – CAS 2025. In press.
[38] Chen H, et al. Advancements and practical considerations for biophysical research: navigating the challenges and future of super-resolution microscopy. Chem. Biomed. Imaging. 2024; 2: 331–344. DOI: 10.1021/cbmi.4c00019.
[39] Aghigh A, et al. Second harmonic generation microscopy: a powerful tool for bio-imaging. Biophys. Rev. 2023; 15: 43–70. DOI: 10.1007/s12551-022-01041-6.
[40] Pleava AM, et al. Holographic microscopy of cell compartments to build realistic models for electric field simulations. Rom. Reports Phys. 2023; 75: 602.
[41] Sandu A-M, et al. Realistic models of cultured cells for electroporation simulations starting from phase images. In: Proc. SPIE, vol. 11718. Advanced Topics in Optoelectronics, Microelectronics and Nanotechnologies X. 2020, p. 117180W.
[42] Nastasa V, et al. Eye tumor tissues imaging with white light diffraction phase microscopy. Rom. Reports Phys. 2022; 74: 604.
[43] Kashyap A, Jain M, Shukla S, Andley M. Role of nuclear morphometry in breast cancer and its correlation with cytomorphological grading of breast cancer: a study of 64 cases. J. Cytol. 2018; 35: 41–45. DOI: 10.4103/JOC.JOC_237_16.
[44] Rogers M, et al. Wavelength and texture feature selection for hyperspectral imaging: a systematic literature review. J. Food Meas. Charact. 2023; 17: 6039–6064. DOI: 10.1007/s11694-023-02044-x.
[45] Einstein AJ, Wu HS, Gil J. Self-affinity and lacunarity of chromatin texture in benign and malignant breast epithelial cell nuclei. Phys. Rev. Lett. 1998; 80: 397-400. DOI: 10.1103/PhysRevLett.80.397.
[46] Siddiqi AM, et al. Use of hyperspectral imaging to distinguish normal, precancerous, and cancerous cells. Cancer. 2008; 114: 13–21. DOI: 10.1002/cncr.23286.

Received October 6, 2025